JPE 5-1-2

Sensorless Control of a PMSM at Low Speeds using High Frequency Voltage Injection

Seok-Chae Yoon* and Jang-Mok Kim†

†*Dept. of Electrical Engineering, Pusan National University
30 Jangjeon-dong Geumjeong-gu, Busan, Korea

ABSTRACT

This paper describes the two control techniques to perform the sensorless vector control of a PMSM by injecting the high frequency voltage to the stator terminal. The first technique is the estimation algorithm of the initial rotor position. A PMSM possesses the saliency which produces the ellipse of the stator current when the high frequency voltage is injected into the motor terminal. The major axis angle of the current ellipse gives the rotor position information at a standstill. The second control technique is a sensorless control algorithm that injects the high frequency voltage to the stator terminal in order to estimate the rotor position and speed. The rotor position and speed for sensorless vector control is calculated by appropriate signal processing to extract the position information from the stator current at low speeds or standstill. The proposed sensorless algorithm using the double-band hysteresis controller exhibits excellent reference tracking and increased robustness. Experimental results are presented to verify the feasibility of the proposed control schemes. Speed, position estimation and vector control were carried out on the floating point processor TMS320VC33.

Keywords: voltage injection, PMSM, sensorless, initial rotor position, low speed

1. Introduction

In recent years the surface mounted permanent magnet synchronous motor (SPMSM or PMSM) has been widely used because of its inherent advantages such as high efficiency, good dynamics and small frame size compared to other motors with the same output[1].

For the vector control of a PMSM, some types of shaft sensors such as optical position encoders or resolvers [2] are fitted to provide a signal that is used to maintain an orthogonal angle between the stator and rotor field in order to produce the maximum torque in the motor. These sensors and the associated signal wirings are significant sources of failure and cost, and add to the overall volume and mass that must be allocated to the motor shaft at the work site. These are the reasons why many authors proposed sensorless control algorithms using different control methods for the estimation of the rotor speed and position.

Researches concerning sensorless PMSM control can be classified into two groups, depending on the speed operating range required by the application: 1) control strategies based on the voltage equation of the motor and 2) control strategies based on signal injection techniques.

Manuscript received July 22, 2004; revised October 4, 2004.
† Corresponding Author: jmok@pusan.ac.kr, Pusan Nat'l University
Tel: +82-51-510-2366, Fax: +82-51-513-0212
*Dept. of Electrical Engineering, Pusan Nat'l University

Control strategies based on the voltage equation can be classified into state observer[3][4], kalman filter[5][6] and voltage model. These methods are preferred for medium or high-speed operation. They require the information of the motor currents and input voltages to estimate the back electromotive force(EMF) which has the information of the rotor position and speed. These methods are very effective, but they depend on the accuracy of the motor parameters. So it is necessary to compensate for the variation in the stator resistance and the back EMF constant caused by the temperature variation. But at low speeds, the magnitude of the back EMF voltage is very small which makes it difficult to detect the motor position and speed.

Signal injection techniques are based on the magnetic saliency of the motor due to the saturation effect or geometric construction. There is no lower limit on the rotor velocity for which these techniques can operate because these methods have are not concerned with the magnitude of the back EMF [7][8] [9] [12-15].

This paper describes sensorless control of a PMSM in at low speeds using a high frequency voltage signal injection. When a high frequency voltage signal is injected into the motor, the stator core around the magnet pole is saturated. This phenomenon results in the magnetic saliency of a PMSM which has the information of rotor position and speed. The proposed sensorless algorithm using the double-band hysteresis control and initial rotor position detection exhibits excellent reference tracking and increased robustness. Also, it does not require the knowledge of any motor parameter and allows low cost implementation. It only requires current sensors already included in standard drives.

2. High Frequency Model of PMSM

The machine model for the PMSM on the d-q synchronous reference frame with an electrical angular velocity ω_r can be represented as follows:

$$v_{ds}^r = R_s i_{ds}^r + L_s \frac{d}{dt} i_{ds}^r - \omega_r L_s i_{qs}^r \tag{1}$$

$$v_{qs}^r = R_s i_{qs}^r + L_s \frac{d}{dt} i_{qs}^r + \omega_r L_s i_{ds}^r + \lambda_m \omega_r \tag{2}$$

where,

R_s, L_s : Stator resistance and stator inductance

v_{ds}^r, v_{qs}^r : d-q axis stator voltages

i_{ds}^r, i_{qs}^r : the stator d-q axis currents

λ_m : the flux linkage of the permanent magnet

If the frequency of the injected voltage is sufficiently high compared to the rotor speed when the machine is operated at low speed, the motor speed can be considered as zero from the point of view of the high frequency component, and there is no output torque ripple. The high frequency component voltage equation can be represented as follows:

$$\begin{bmatrix} v_{dsi}^r \\ v_{qsi}^r \end{bmatrix} = \begin{bmatrix} R_s + j\omega_i L_s & 0 \\ 0 & R_s + j\omega_i L_s \end{bmatrix} \begin{bmatrix} i_{dsi}^r \\ i_{qsi}^r \end{bmatrix} \tag{3}$$

where, v_{dsi}^r, v_{qsi}^r, i_{dsi}^r, i_{qsi}^r are high frequency components of the stator voltages, currents in the d-q axis and ω_i is the frequency of the injected voltage.

It is possible to observe that at sufficiently high ω_i, $R_s + j\omega_i L_s$ can be approximately reduced to $j\omega_i L_s$.

When the flux of the magnet poles aligns with the flux of the stator, the resultant flux is very large, and magnetically saturates the stator iron. This magnetic saturation makes the electric saliency so that the q-axis inductance becomes slightly larger than that of the d-axis.

From the above reasoning, (3) can be reduced to (4).

$$\begin{bmatrix} v_{dsi}^r \\ v_{qsi}^r \end{bmatrix} = \begin{bmatrix} j\omega_i L_{ds} & 0 \\ 0 & j\omega_i L_{qs} \end{bmatrix} \begin{bmatrix} i_{dsi}^r \\ i_{qsi}^r \end{bmatrix} \tag{4}$$

where L_{ds}, L_{qs} are d, q axis inductances.

Fig. 1 shows the relationship between an actual d-q axis and the estimated d-q axis. The estimation error of the rotor position is θ_{err} as shown in Fig.1, and the relationship of the stator voltages and currents between in an actual d-q axis and in the estimated d-q axis is derived like (5) and (6).

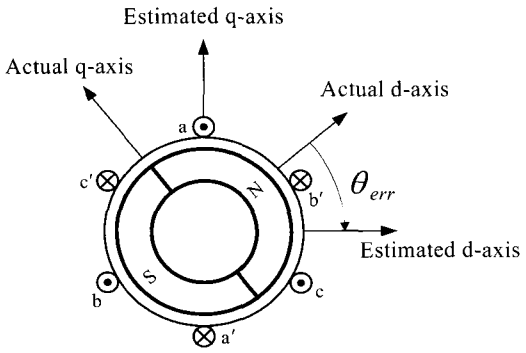

Fig. 1 Actual d-q axis s and estimated d-q axis

$$\begin{bmatrix} v_{dsi}^r \\ v_{qsi}^r \end{bmatrix} = \begin{bmatrix} \cos\theta_{err} & -\sin\theta_{err} \\ \sin\theta_{err} & \cos\theta_{err} \end{bmatrix} \begin{bmatrix} \hat{v}_{dsi}^r \\ \hat{v}_{qsi}^r \end{bmatrix} \quad (5)$$

$$\begin{bmatrix} i_{dsi}^r \\ i_{qsi}^r \end{bmatrix} = \begin{bmatrix} \cos\theta_{err} & -\sin\theta_{err} \\ \sin\theta_{err} & \cos\theta_{err} \end{bmatrix} \begin{bmatrix} \hat{i}_{dsi}^r \\ \hat{i}_{qsi}^r \end{bmatrix} \quad (6)$$

where, $\hat{v}_{ds}^r$, $\hat{v}_{ds}^r$, $\hat{i}_{ds}^r$, $\hat{i}_{ds}^r$ are the stator voltages and currents in the estimated synchronous reference frame.

From (4), (5), and (6) the high frequency component of the stator current in the estimated synchronous reference frame is derived as follows:

$$\hat{i}_{dsi}^r \cong j\frac{a+b\cos 2\theta_{err}}{c}\hat{v}_{dsi}^r + j\frac{b\sin 2\theta_{err}}{c}\hat{v}_{qsi}^r \quad (7)$$

$$\hat{i}_{qsi}^r \cong j\frac{b\sin 2\theta_{err}}{c}\hat{v}_{dsi}^r + j\frac{a+b\sin 2\theta_{err}}{c}\hat{v}_{qsi}^r \quad (8)$$

where, $a=(L_{qs}+L_{ds})$, $b=(L_{qs}-L_{ds})$,

and $c=2\omega_i L_{ds}L_{qs}$

3. Pre-Processor

The pre-processor is used to extract θ_{err} from the high frequency component of the stator q-axis current in the estimated synchronous reference frame. Fig. 2 shows the block diagram of a pre-processor[10].

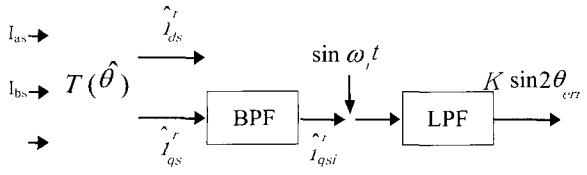

Fig. 2 Block diagram of a pre-processor

If the high frequency voltage is injected as in (9), the high frequency component of the stator current in the estimated synchronous reference frame can be represented as (10), and (11).

$$\begin{bmatrix} \hat{v}_{dsi}^r \\ \hat{v}_{qsi}^r \end{bmatrix} = v_{si}\begin{bmatrix} \cos(\omega_i t) \\ 0 \end{bmatrix} \quad (9)$$

$$\hat{i}_{dsi}^r \cong v_{si}\sin\omega_i t\left(\frac{L_{qs}+L_{ds}+a\cos 2\theta_{err}}{c}\right) \quad (10)$$

$$\hat{i}_{qsi}^r \cong v_{si}\sin\omega_i t\left(\frac{b\sin 2\theta_{err}}{c}\right) \quad (11)$$

From (11) the input signal related with the estimation error of the rotor position can be obtained via the signal demodulating process in (12).

$$LPF[\hat{i}_{qsi}^r \times \sin\omega_i t] \cong \frac{v_{si}(-b)}{2c}\sin 2\theta_{err} \cong K\sin 2\theta_{err} \quad (12)$$

where, $K=\frac{v_{si}(-b)}{2c}$

From the assumption that $\theta_{err} \cong 0$, and $\sin 2\theta_{err} \cong 2\theta_{err}$ the output of the pre-processor in (12) can be reduced to (13).

$$LPF[\hat{i}_{qsi}^r \times \sin\omega_i t] \cong K2\theta_{err} \quad (13)$$

4. Sensorless Control Strategy

4.1 Rotor Position Detection at standstill

Because the characteristic of the sine function there can be uncertainty between $\frac{\pi}{4}$ and $\frac{7\pi}{4}$ as shown in Fig.3. Within this region the sensorless vector control is not guaranteed by using the sensorless control algorithm already mentioned above in Section III. The estimation algorithm of the initial rotor position is necessary for solving this problem.

When the balanced 3-phase and high frequency voltages are injected to the stator terminals, the stationary d-q axis currents make the ellipse due to the saturation effect of the PMSM as shown in Fig. 4. The information of the complete one cycle current is needed in order to

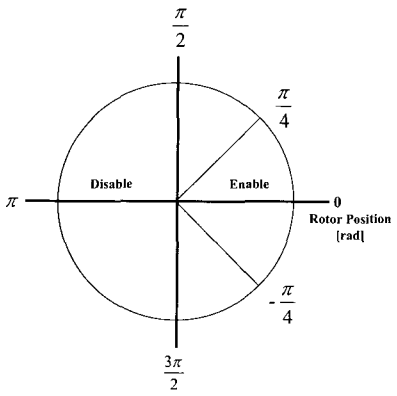

Fig. 3 Initial starting region, depending upon the position of the rotor

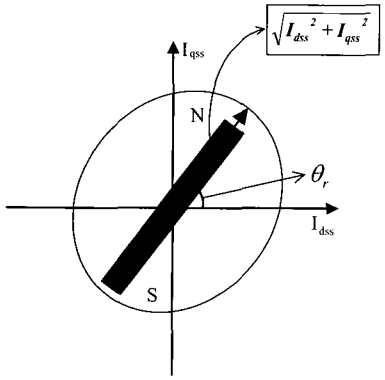

Fig. 4 Current ellipse in the stationary reference frame

make a complete ellipse and to estimate the rotor position by injecting the high frequency voltage to the stator terminal. This is due to the major axis angle of the stator current gives the direct information of the rotor position as shown in Fig. 4.

Fig. 5 shows the phenomenon of the magnetic saturation according to the rotor position.

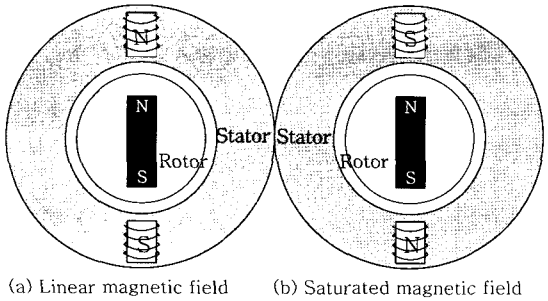

(a) Linear magnetic field (b) Saturated magnetic field

Fig. 5 Magnetic saturation effect according to the rotor position

Fig. 6 shows the flow chart to estimate the initial rotor position estimation.

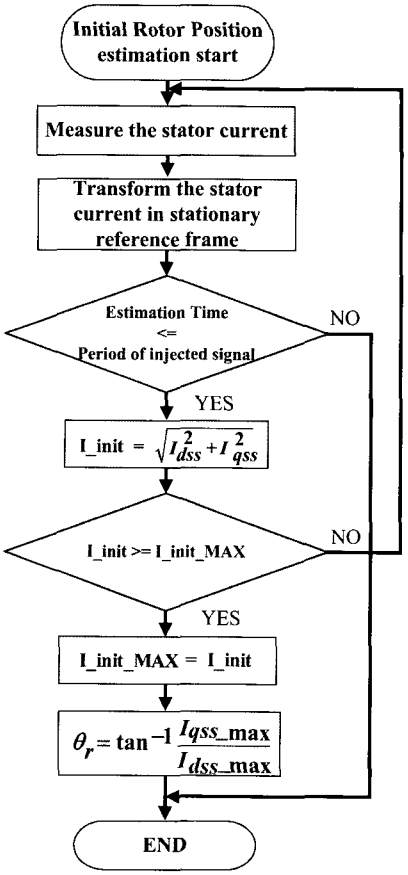

Fig. 6 Flow chart of the initial rotor position estimation

4.2 Double Band Hysteresis Control

Fig. 7 shows the concept of the conventional Bang-Bang control. When the rotor position estimation error falls below zero, the output of the Bang-Bang controller is $-\theta_u$, and when the rotor position estimation error rises above zero, the output is θ_u.

Fig. 8 shows the concept of the double-band five-level hysteresis control. The estimation error of the rotor position is usually limited within the inner band because in the steady state the estimation error of the rotor position is very small. The output of the double-band five-level hysteresis controller can be determined within several levels, and has less of a ripple component compared to the Bang-Bang controller.

Therefore the proposed controller has several attractive

features when compared to the bang-bang controller. The double-band five-level hysterisis controller is more stable, yields a more dynamic performance and has a smaller estimation error in the steady state.

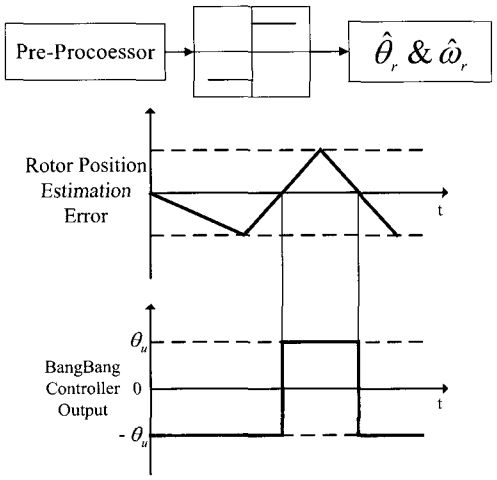

Fig. 7 Conventional Bang-Bang Control

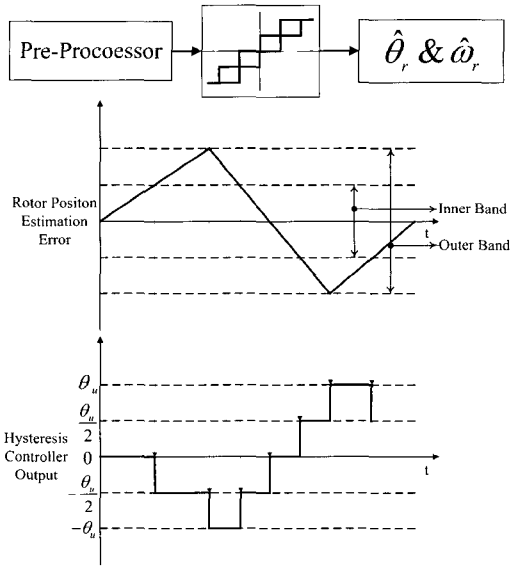

Fig. 8 Proposed double-Band 5-Level Hysteresis Control

Fig. 9 shows the block diagram of the proposed two sensorless control algorithms including the initial rotor position estimation at standstill and the sensorless vector control. At first the algorithm of the initial rotor position estimation functions, and then at low speeds the sensorless vector conrol begins functioning.

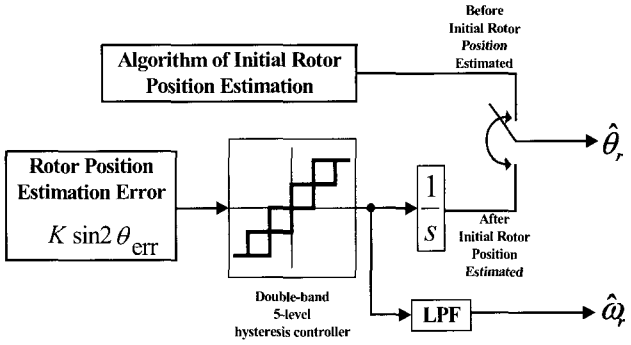

Fig. 9 Block diagram of the proposed sensorless control algorithms

5. Experimental Results

The experimental setup was utilized to verify the usefulness of the proposed two control algorithms. Table 1 shows the nominal parameters of the PMSM for the experiments.

Table 1 Nominal Parameters of PMSM

Rated voltage	220[V]	Poles	48
Rated current	9[A]	Stator registor	4.1[Ω]
Rated speed	600[rpm]	Stator reactance	20[mH]
Maximum speed	2000[rpm]	backEMF constant	0.083[V/rad/s]

Fig. 10 shows the control block diagram of the sensorless drive system of the PMSM including the proposed two algorithms. The sampling time of the current regulator is 62.5μsec. The switching frequency of the PWM inverter is 8 kHz. The space vector PWM algorithm is used for maximum utilization of DC link voltage. All programs are implemented with a 32bit floating point microprocessor, DSP TMS320VC33 made by TI. The frequency of the injected voltage is 355Hz and the amplitude is 60V. While the amplitude of the injected voltage is not small, the frequency is so high that it has no effect on the output torque. After the motor speed reaches the point where there is enough back EMF, other sensorless control algorithms (which have been developed by many previous authors) can be applied to the sensorless drive system for operation at high speeds [1][4].

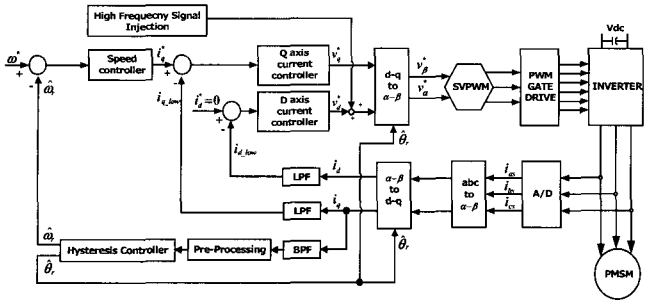

Fig. 10 Sensorless control block diagram of PMSM

IIn Fig. 11 the rotor is located at 0.05[rad] electrical degrees. The stationary d-q currents and its ellipse are shown in Fig. 11, 12, and 13 when the high frequency voltage is injected to the stator terminal to estimate the initial rotor position at a standstill. The initial rotor position is easily determined from the major axis angle of the ellipse as shown in Fig. 11, 12, and 13.

In Fig. 12 and Fig. 13 the conditions are the same as in Fig. 11 except for the rotor position. From successive tests, the position error of the rotor is acquired within ± 15 electrical degree.

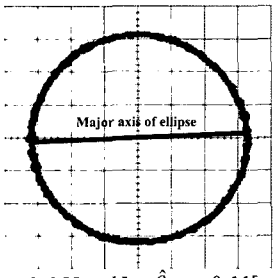

$\theta_r = 0.05[rad]$ $\hat{\theta}_r = -0.11[rad]$

$\theta_{err} = -9.33[^\circ]$

Fig. 11 In case of the rotor initial position 0.05[rad] at standstill

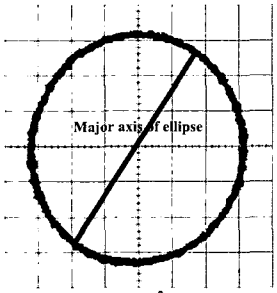

$\theta_r = -1.97[rad]$ $\hat{\theta}_r = -2.06[rad]$

$\theta_{err} = -5.48[^\circ]$

Fig. 12 In case of the rotor initial position -1.97[rad] at standstill

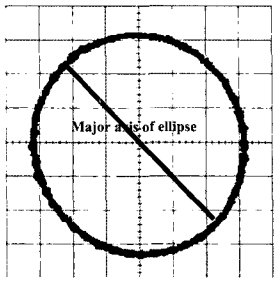

$\theta_r = -0.85[rad]$ $\hat{\theta}_r = -0.92[rad]$

$\theta_{err} = -4.39[^\circ]$

Fig. 13 In case of the rotor initial position -0.85[rad] at standstill

Fig. 14 shows the estimated initial rotor position during start-up without the estimation algorithm of the initial rotor position. Due to the uncertainty of 90 degrees of pre-processor output, the estimated rotor position does not track the actual rotor position.

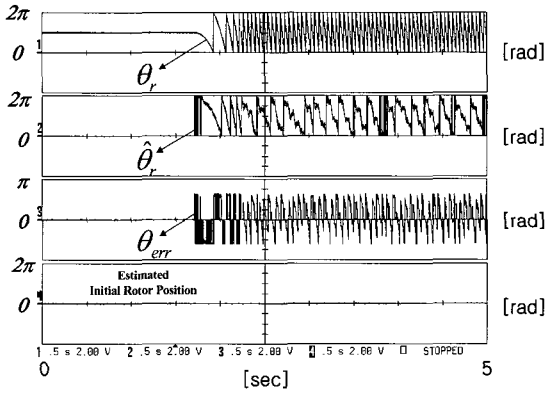

Fig. 14 Estimated position during start-up without initial rotor position estimation (Speed reference: 10[rpm])

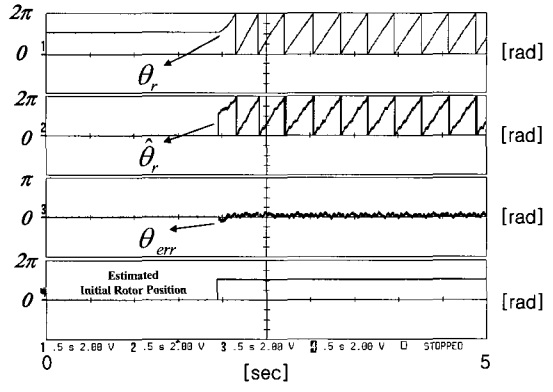

Fig. 15 Estimation rotor position of the proposed sensorless algorithms including the initial rotor position estimation algorithm (Speed reference: 10[rpm])

Fig. 15 shows the estimated rotor position of the proposed sensorless algorithms during start-up. After estimating the initial rotor position, the estimated rotor position, adapting the proposed sensorless algorithm, begins tracking the actual rotor position as shown in Fig. 15.

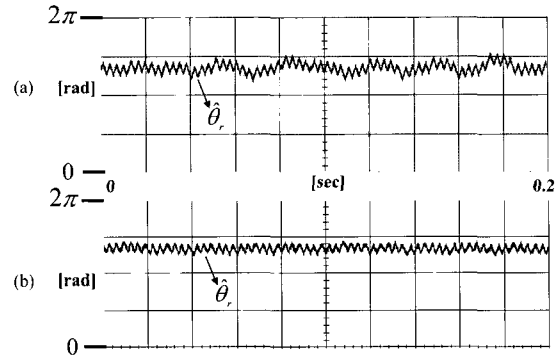

Fig. 16 Estimated position in case of the rotor position 4.24[rad](Speed reference: 0[rpm])
(a) Bang-Bang Control
(b) Double-Band hysteresis control

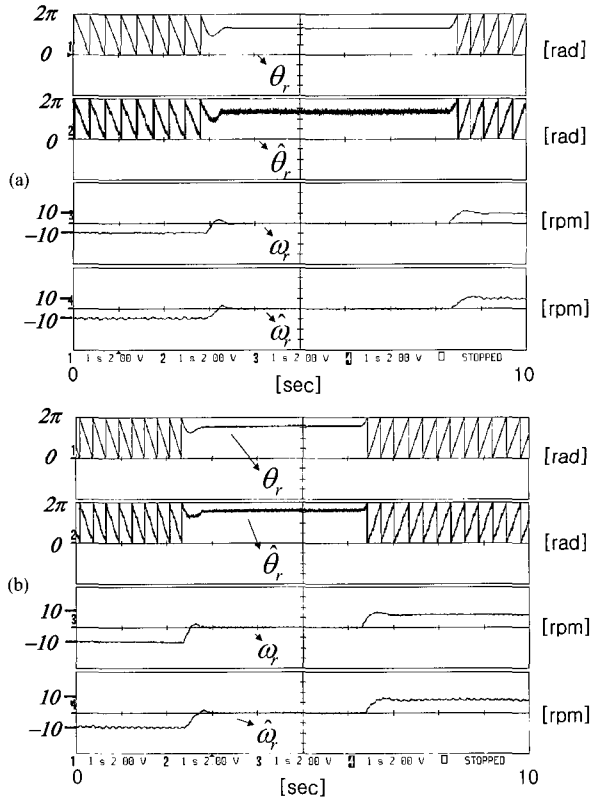

Fig. 17 Step speed response(Speed reference: -10 → 0 → 10 [rpm])
(a) Bang-Bang Control
(b) Double-Band hysteresis Control

For the purpose of performance comparison, the control using the conventional Bang-Bang and the proposed Double-Band hysteresis control method have been monitored, and the experimental waveforms are as shown in Fig. 16 when the speed reference is 0[rpm]. As shown in Fig. 16 the conventional Bang-Bang controller produces the larger amplitude of the harmonic position.

The conditions in Fig. 17 and Fig. 18 are the same as for Fig. 16 except for the speed reference. The double-band hysteresis control shows small ripple components compared to the Bang-Bang control, and good reference tracking. The proposed scheme gives a good speed and position estimation even at low speeds. The speed estimation error is very small due to the injection the high frequency voltage.

Based on the experimental results, it is apparent that the proposed sensorless control algorithm performs much better than the conventional sensorless control algorithm.

6. Conclusions

In this paper, two estimation algorithms which calculate the initial rotor position at standstill and a sensorless vector control algorithm are proposed to control a PMSM without a mechanical speed sensor. The estimation concept used to calculate the initial rotor position at standstill is based upon the saturation effect of the rotor. To estimate the initial rotor position and identify the rotor magnet N-S polarity, high frequency voltage (355Hz) is injected to the stator terminal. The rotor position is calculated from the major axis angle of the stator current ellipse.

For the sensorless vector control of a PMSM the rotor position is estimated by injecting high frequency voltage to the stator terminal. No machine parameters are used in these sensorless algorithms so resistance to motor parameters variation is guaranteed. Moreover, the double-band hysteresis control has several attractive features including good reference tracking, dynamic performance and small ripple components when compared to the conventional Bang-Bang control. Also vector control performs very well even at low speeds and standstill. The experimental results show the usefulness of the two proposed algorithms for the sensorless vector

control of a PMSM.

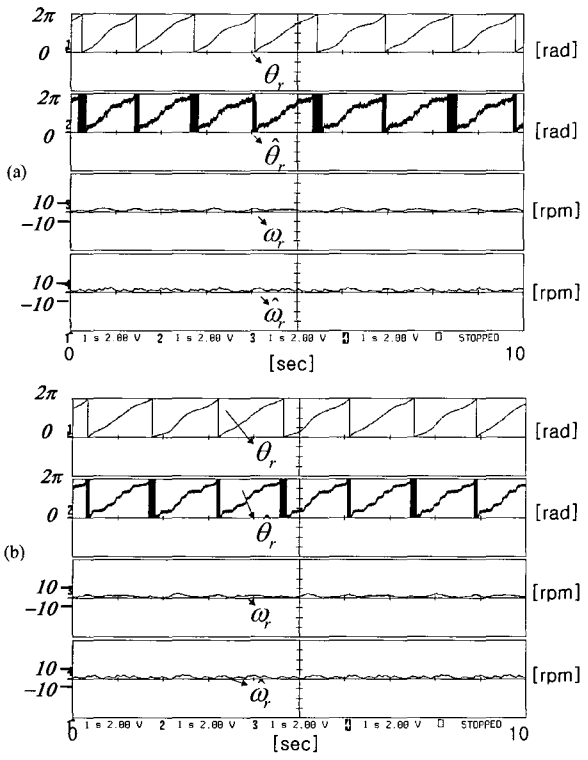

Fig. 18 Step speed response (Speed reference: 2 [rpm])
(a) Bang-Bang Control
(b) Double-Band hysteresis Control

References

[1] J.S.Kim, S.K.Sul. "High performance PMSM drives without rotational position sensor using reduced order observer" IEEE 1995 IAS Annual Meeting, pp.75-82.

[2] Synchro/Resolver conversion handbook, DDC, 1994

[3] R.B.Sepe et al, "Real-Time Observer-Based (Adaptive) Control of a Permanent-Magnet Synchronous Motor without Mechanical Sensor," IEEE Trans. Ind. Appl., vol.28, no.6, pp.1345-1352 ,1992.

[4] L.A.Jones, J.H.Lang "A State Observer for the Permanent Magnet Synchronous Motor",IEEE Trans. Ind. Electronics, vol.36, no.3, August 1989, pp.374-382.

[5] A. Bado. et al., "Effective estimation of speed and rotor position of a PM synchronous motor drive by a Kalman filtering technique," in Proc. IEEE PESC'92, pp.951-957, 1992.

[6] R. Dhaouadi. N.Mohan. L.Norum, "Design and Implementation of an Extended Kalman Filter for the State Estimation of a Permanent Magnet synchronous Motor", IEEE Trans. On Power Electronics, Vol.6, No.3, July 1991, pp 497-497.

[7] M.J.Corley and R.D.Lorenz, "Rotor position and velocity estimation for a salient-pole permanent magnet synchronous machine at standstill and high speeds," IEEE Trans. on Industry Applications, Vol. 34, No.4, pp. 36-41, July/Aug 1998.

[8] J.I.Ha, S.K.Sul, "Sensorless Field-Orientation Control of an Induction Machine by High-frequency Signal Injection," IEEE Trans. on Ind. Appl., Vol.35, No.1, pp.45-51,1999.

[9] J.H.Jang, S.K.Sul, J.I.Ha, K.Ide, M.Sawamura, "Sensorless Drive of SMPM Motor by High Frequency Signal Injection" IEEE Trans. on Ind. Appl., Vol.39, No.1, pp.1031-1039,2003.

[10] J.H.Jang, J.I.Ha, S.K.Sul, "Vector control of surface-mounted permanent magnet motor without any rotational transducer" IEEE APEC, Vol.2, pp.845-849,2001

[11] J.I.Ha, Ohto M., J.H.Jang, S.K.Sul, "Design and selection of AC machines for saliency-based sensorless control" IEEE-IAS Conf. Rec., Vol.2, pp.1155 ~ 1162, 2002.

[12] P.L.Jansen and R.D.Lorenz, "Transducerless field orientation concepts employing saturation-induced saliencies in induction machines.", IEEE-IAS Conf. Rec., Vol.1, pp.174 ~ 181, 1995.

[13] P.L.Jansen, R.D.Lorenz, D.W.Novotny, "Observer-Based Direct Field Orientation; Analysis and Comparison of Alternative Methods", IEEE Trans. on Ind. Appl, Vol.30, pp. 945-953, 1994.

[14] Consoli, A.; Scarcella, G.; Testa, A., "Industry application of zero-speed sensorless control techniques for PM synchronous motors ", IEEE Trans. on Ind. Appl, Vol.37, pp.513-521, 2001.

[15] J.M.Kim, S.J.Kang, S.K.Sul; "Vector control of interior permanent magnet synchronous motor without a shaft sensor", IEEE APEC Conf Vol.2, pp.743-748, 1997.

Seok-Chae Yoon was born in Busan, Korea in 1979. He received the B.S. and M.S. degree in electrical engineering from Pusan National University, Korea, in 2002 and 2004, respectively. Since 2004, he has been with the computer systems division of Samsung

Electronics. His research interests are in the areas of sensorless control of ac motors and micro processors.

Jang-Mok Kim was born in Pusan, Korea, in August 1961. He received the degree in electrical engineering from Pusan National University in 1988, and M.S. and Ph.D degree from Seoul National University, Korea, in 1991 and 1996, respectively. He is presently working toward the Ph.D. degree at Seoul National University. He joined Korea Electrical Power research institute as a senior research engineer from 1997 to 2000. Since 2001, he has been a faculty member in the division of Electrical and Electronics Engineering at Pusan National University, serving as an assistant professor. He is a research member of the research institute of Computer Information and Communication at Pusan National University. His present interests are in power electronic control of electric machines and power quality.